Extended Abstract DOI: https://doi.org/10.64862/ajeg.2025.2sp.27.123 Open Access

Regional-Scale Inventory of Liquefaction Triggered by the 2025 Mw 7.7 Mandalay Earthquake, Myanmar

Sotiris Valkaniotis[1], George Papathanassiou[1*], Janusz Wasowski[2], Maria Taftsoglou[3] and Ranjan Kumar Dahal[4]

[1]School of Geology, Aristotle University of Thessaloniki, Greece
[2]CNR-IRPI National Research Council – Research Institute for Geo-hydrological Protection, Bari, Italy
[3]Department of Earth Sciences, University of Ferrara, Italy
[4]Central Department of Geology, Tribhuvan University, Kirtipur, Kathmandu, Nepal

(*Corresponding E-mail: gpapatha@geo.auth.gr)

Received: August 8, 2025, Accepted: October 15, 2025

Abstract: On March 28, 2025, a M_w 7.7 earthquake ruptured a ~500 km segment of the strike-slip Sagaing Fault in central Myanmar. The earthquake produced widespread structural damage and co-seismic ground failures, including extensive liquefaction and lateral spreading. This study presents the first systematic mapping and analysis of earthquake-induced liquefaction associated with the 2025 Mandalay earthquake, using medium resolution Copernicus Sentinel-2 satellite imagery acquired shortly after the earthquake. We identified over 18,000 liquefaction sites within an area of more than 80,000 km^2, with the highest concentrations along the Irrawaddy and Sittang River valleys, in vicinity to the fault rupture. Liquefaction predominantly occurred in Holocene fluvial deposits, including meandering channels, floodplains, and abandoned paleochannels, reflecting the influence of geomorphology and sediment characteristics. Over 95% of the sites were located within 20 km of the fault rupture. Our results demonstrate the importance of integrating geomorphic, lithological, and seismic parameters into regional-scale assessments of seismic hazard.

Keywords: ***Co-seismic ground failure, Liquefaction, Satellite-based mapping, Sentinel-2, Myanmar, Geomorphology.***

Introduction

On March 28, 2025, a large magnitude earthquake (M_w 7.7) hit central Myanmar (formerly Burma) at 12:50 p.m. local time (USGS, 2025).

The shallow depth (~10 km) of the mainshock epicenter resulted in extreme ground shaking (Modified Mercalli Intensity IX–X) in the Mandalay Region (USGS, 2025). The 2025 Mandalay earthquake ruptured a major segment of the right-lateral strike-slip Sagaing Fault and triggered many ground failures including landslides, surface ruptures, liquefaction and lateral spreading (Figure 1). Strong earthquakes occurred in the past along the Sagaing Fault zone, with reports of liquefaction dating back to 1839.

Methodology

We used Copernicus Sentinel-2 multispectral imagery acquired after the event (30 March – 4 April 2025) to identify and map liquefaction triggered by the 28 March 2025 earthquake.

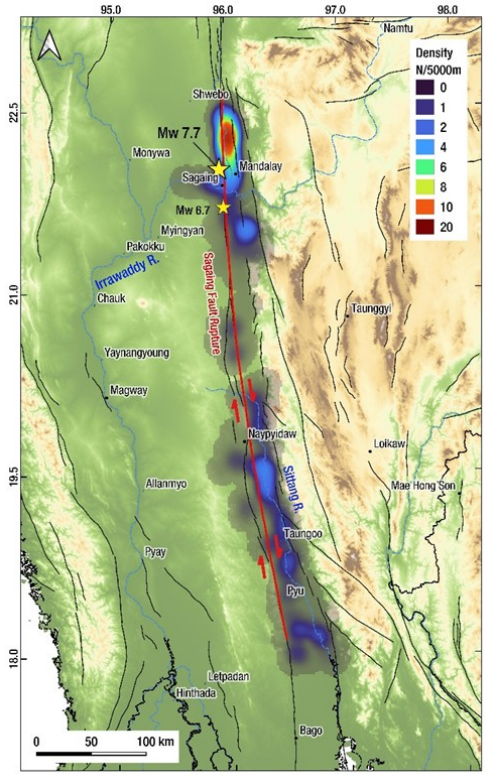

Figure 1, Overview map of the 2025 fault rupture (red) and density of mapped liquefaction sites.

Based on our previous experiences in rapid reconnaissance mapping of liquefaction phenomena (Papathanassiou et al., 2022; Taftsoglou et al., 2023), we targeted our research using the mapped fault surface trace focusing on the area roughly enclosed by the 0.1 g peak ground acceleration (PGA) contour. We also exploited co-seismic displacement maps that we

developed from Copernicus Sentinel-2 imagery, and InSAR co-seismic pairs from Copernicus Sentinel-1 SAR imagery. Using available regional-scale geological maps, we delineated the Holocene and late Quaternary surficial geological formations. Mapping of liquefaction was performed manually and accomplished within a period of one week, using the inspection and focus methodology (cf., Taftsoglou et al., 2023). Liquefaction sites were mapped as points representing either individual features or clusters of multiple liquefaction features (Figure 2). Visual identification of earthquake-induced liquefaction phenomena was based on the characteristic features, light grey color sites. We used change detection techniques (band differencing) for assistance during visual mapping. The detected liquefaction features included mostly fissures, circular sand boils/craters, and ejecta along surface ruptures or ground cracks, isolated or in complex groups. We also identified surface deformations caused by lateral spreading and ground oscillation. Liquefaction mapping was validated using available very high-resolution satellite imagery in selected locations and post-earthquake field reports.

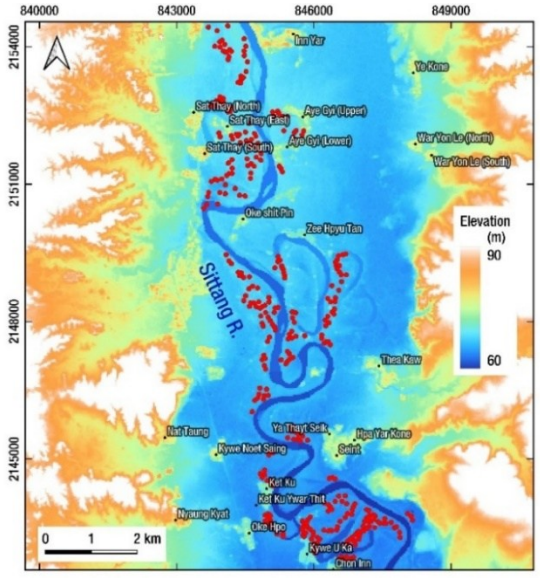

Figure 2, Liquefaction sites (red dots) mapped along the Sittang meandering river valley. Elevation from Copernicus DEM 30.

Result and conclusion

We identified 18,063 liquefaction and lateral spreading sites along a 520 km long section of the Sagaing Fault. Most liquefaction-related phenomena were concentrated along meandering river valleys, abandoned strands or avulsions of rivers, drained lake basins and swamps, and river coastal areas.

The highest density of liquefaction sites was in the epicentral area along the Irrawaddy River, north of Mandalay and along the valley of Sittang River. Our results reinforce a growing body of international literature (e.g., Civico et al., 2015; Villamor et al., 2016; Bastin et al., 2018; Papathanassiou et al., 2022) indicating that the spatial distribution of liquefaction is strongly influenced by fluvial and alluvial geomorphic settings, particularly those containing Holocene-age sediments. About 95% of the liquefaction sites were within 20 km from the fault rupture and more than 95% of liquefaction manifestations are within the areas of PGA ≥ 0.4 g and PGV ≥ 60 cm/sec. Our results show that for the 2025 Mw 7.7 Mandalay earthquake, the distance from the surface fault rupture is a more effective predictor of the spatial extent of liquefaction phenomena than the distance from the mainshock epicenter.

References

Bastin, S., Odgen, M., Wotherspoon, L. M., van Ballegooy, S., Green, R. A., and Stringer, M. (2018). Geomorphological influences on the distribution of liquefaction in the Wairau Plains, New Zealand, following the 2016 Kaikōura earthquake. Bulletin of the Seismological Society of America, 108(3), 1683–1694. https://doi.org/10.1785/0120170248

Civico, R., Brunori, C. A., De Martini, P. M., Pucci, S., Cinti, F. R., and Pantosti, D. (2015). Liquefaction susceptibility assessment in fluvial plains using airborne lidar: The case of the 2012 Emilia earthquake sequence area (Italy). Natural Hazards and Earth System Sciences, 15(11), 2473–2483. https://doi.org/10.5194/nhess-15-2473-2015

Papathanassiou, G., Valkaniotis, S., Ganas, A., Stampolidis, A., Rapti, D., and Caputo, R. (2022). Floodplain evolution and its influence on liquefaction clustering: The case study of the March 2021 Thessaly, Greece, seismic sequence. Engineering Geology, 298, 106542. https://doi.org/10.1016/j.enggeo.2022.106542

Taftsoglou, M., Valkaniotis, S., Papathanassiou, G., and Karantanellis, E. (2023). Satellite imagery for rapid detection of liquefaction surface manifestations: The case study of Türkiye–Syria 2023 earthquakes. Remote Sensing, 15(17), 4190. https://doi.org/10.3390/rs15174190

U.S. Geological Survey. (2025). Overview of the M 7.7 – 2025 Mandalay, Burma (Myanmar) earthquake. U.S. Department of the Interior. Available at: https://earthquake.usgs.gov/earthquakes/eventpage/us7000pn9s/executive

Villamor, P., Almond, P., Tuttle, M. P., Giona-Bucci, M., Langridge, R. M., Clark, K., Ries, W., Bastin, S. H., Eger, A., Vandergoes, M., Newnham, R., and Rhoades, D. A. (2016). Liquefaction features produced by the 2010–2011 Canterbury earthquake sequence in southwest Christchurch, New Zealand, and preliminary assessment of paleo liquefaction features. Bulletin of the Seismological Society of America, 106(4), 1747–1771. https://doi.org/10.1785/0120150223